Fuel Processing Technology 226 (2022) 107092

Contents lists available at ScienceDirect

Fuel Processing Technology

journal homepage: www.elsevier.com/locate/fuproc

Research article

Conversion of aqueous ethanol/acetaldehyde mixtures into 1,3-butadiene over a mesostructured Ta-SBA-15 catalyst: Effect of reaction conditions and kinetic modelling

G.M. Cabello González [a], A.L. Villanueva Perales [a,*], A. Martínez [b], M. Campoy [a], F. Vidal-Barrero [a]

[a] Departamento de Ingeniería Química y Ambiental, Escuela Técnica Superior de Ingeniería, Universidad de Sevilla, Camino de los Descubrimientos, s/n., 41092 Sevilla, Spain

[b] Instituto de Tecnología Química, Universitat Politècnica de València-Consejo Superior de Investigaciones Científicas (UPV-CSIC), Avda. de los Naranjos s/n, 46022, Valencia, Spain

ARTICLE INFO

Keywords:
Ethanol
1,3-butadiene
Ostromislensky process
Kinetic model
Ta-SBA-15 catalyst

ABSTRACT

This paper studies key issues for the design of industrial ethanol to 1,3-butadiene two-step processes, focusing on the second catalytic reaction step, for which a Ta-SBA-15 catalyst was chosen as a representative of the new generation of two-step catalysts. The important practical aspects studied were: i) the effect of operating conditions and the presence of impurities (water) in the ethanol feedstock on the performance of the catalyst, ii) stability and regeneration of the catalyst, and iii) the development of a kinetic model that can be used as a tool for designing the industrial process. The results showed that there are large non-linear interacting effects between the reaction conditions (temperature, space velocity and ethanol/acetaldehyde mole ratio) which must be carefully selected to optimize the catalyst performance. When shifting from an anhydrous to an aqueous ethanol/acetaldehyde feed (7.5 wt% water), catalyst performance at high temperature barely changed while at low temperature, conversion of ethanol and acetaldehyde decreased. Water in the feed largely increased the stability of Ta-SBA-15 catalyst. Finally, a kinetic model of a fresh catalyst was developed, whose novelty lies in the use of kinetic equations that account for the effect of water in the feed on the catalyst performance.

1. Introduction

1,3-Butadiene is a key monomer in the production of numerous artificial elastomers used widely in the industry. Presently, it is mostly produced as a byproduct in the manufacture of ethene by steam cracking of oil-derived naphtha. In the search of a more environmentally production of 1,3-butadiene, encouraged by the new environmental policies [1,2], there has been a renewed interest in abandoned industrial processes where bioethanol was used as feedstock. From 1920 to 1960 the Lebedev process (one-step process) and the Ostromislensky process (two-step process) operated in the USSR and USA, respectively. In the Ostromislensky process ethanol is partially dehydrogenated into acetaldehyde over a first catalyst and then the ethanol/acetaldehyde mixture is further transformed into 1,3-butadiene over a second catalyst [3]. In the one-step process all these transformations take place over a single catalyst [4]. As the ethanol dehydrogenation to acetaldehyde has been widely studied [5–11], this study will focus on the second reaction stage of the two-step process.

The most accepted conversion pathway of acetaldehyde/ethanol mixtures into 1,3-butadiene is the Toussaint-Kagan pathway [12–20], which comprises the following reaction steps: i) aldol-condensation of acetaldehyde to crotonaldehyde, ii) Meerwein-Ponndorf-Verley-Oppenauer (MPVO) reduction of crotonaldehyde with ethanol to crotyl alcohol, co-producing acetaldehyde for the previous step, and iii) dehydration of crotyl alcohol to produce 1,3-butadiene. Overall, one molecule of acetaldehyde reacts with one molecule of ethanol to yield one molecule of 1,3-butadiene and two molecules of water. By the mid of the 20th century, scientists of the Carbide and Carbon Chemical Corporation [21] and the Mellon Institute [22] found that silica-supported catalysts containing oxides of transition metals of groups 4 and 5, namely, Ta, Hf, Zr and Nb were very active for the conversion of mixtures of acetaldehyde/ethanol into 1,3-butadiene. The Lewis acid sites

* Corresponding author.
E-mail address: angelluisvp@us.es (A.L. Villanueva Perales).

https://doi.org/10.1016/j.fuproc.2021.107092
Received 31 July 2021; Received in revised form 18 October 2021; Accepted 7 November 2021
Available online 14 November 2021

(LAS) related to these transition metals promote the acetaldehyde aldol condensation and MPVO reduction of crotonaldehyde [18,23,24]. In addition, the acidity of the silica support has been found to play an important role [23], probably related to the crotyl alcohol dehydration step. However, a subtle tuning of catalyst acidity is needed to prevent as much as possible the unwanted dehydration of ethanol to ethene and diethyl ether and polycondensation of acetaldehyde to heavy products [25].

The industrial two-step process commercialized by the Carbide and Carbon Chemical Corporation in USA used 2 wt% tantalum oxide supported on silica-gel as catalyst for the second reaction stage [22,26]. In the last decade, a new generation of two-step catalysts has been developed to improve the performance of the industrial catalyst. Some authors have studied new silica supports with higher surface area for tantalum oxide, such as ordered mesoporous silica (OMS) [27], which, by proper adjustment of pore size and primary particle size of the support, facilitates diffusion of reactants and products and dispersion of tantalum oxide. These improvements result in catalysts displaying from 2 to 5 times greater 1,3-butadiene productivity and better coking tolerance than the industrial catalyst. Introduction of isolated Ta(V) atoms in the framework of SiBEA zeolites also resulted in very selective catalysts (up to 90%) [28]. Most authors have focused on developing catalysts using Zr, which is an element most abundant and cheaper than Ta, but with a slightly lower activity for this reaction [22]. Again, the influence of the type and properties of the silica support have been thoroughly studied in the case of Zr-containing catalysts [25,29–31] as well as the content of Zr [25,29,32,33] and synthesis method [25,32,34], with the aim to enhance intra-particle mass transfer and availability of Zr-related LAS. High selective catalysts (>70%) were found when zirconium species were dispersed on mesocellular siliceous foam (MCF) [29], OMS and Nano-SiO_2 [25,30,31] and all-silica MFI zeolite nanosheets doped with Mg [33]. Finally, alkali-exchanged BEA zeolites doped with MgO were also found to be highly selective, without the need of any transition metal [35].

Unlike the development of selective catalysts for the second reaction stage, practical aspects of their industrial application, such as the effect of operating conditions and the presence of impurities in the reactant feed on catalyst performance, have not been studied thoroughly. In the recent literature on two-step catalysts, operating conditions (temperature, space velocity and ethanol/acetaldehyde mole ratio) have been usually examined one at a time, therefore neglecting possible interacting effects [25,29,32–34]. Because of this, some apparently contradictory results have been reported recently. For instance, Cheong et al. [29] and Li et al. [33] reported that 1,3-butadiene selectivity had a maximum with temperature while Kyriienko et al. [28] and Yang et al. [25] reported a steady decline in selectivity with temperature. In another instance, Han et al. [34] and Xu et al. [32] reported a low sensitivity of 1,3-butadiene selectivity to space velocity while Yang et al. [25] reported a maximum with space velocity. The importance of the interacting effects was patent for the industrial two-step catalyst when Corson et al. [37] searched for optimal operating conditions to maximize 1,3-butadiene yield. They found that, keeping constant space velocity, the optimal ethanol/acetaldehyde mole ratio (ETOH/AC) that maximized 1,3-butadiene yield changed with temperature, which also occurred to the optimal space velocity when keeping constant the ETOH/AC ratio. Therefore, the effect of operating conditions on the performance of the new generation of catalysts must be evaluated carefully. Furthermore, the effect of impurities in the reactant feed should not be disregarded. Of those, the most important is water, which might be present in the ethanol feedstock, but is also produced in the 1,3-butadiene reaction. The industrial two-step process used azeotropic ethanol as feedstock (~7.5 wt% H_2O) [22], and therefore, the ethanol/acetaldehyde mixture fed to the second reactor contained almost the same mass content of water. For the industrial two-step catalyst, water was found to lower 1,3-butadiene productivity and, in a lesser extent, catalyst deactivation [26]. These effects of water have been recently reported for one-step catalysts in addition to promotion of unwanted ethanol dehydration to ethene and diethyl ether [38–44]. However, unlike for one-step catalysts [43] a thorough study of the effect of water for different operation conditions on catalyst performance has not been conducted for two-step catalysts. This type of study is important because, when designing a two-step process, an optimum water content in the reactor feed should be chosen to find a trade-off between the impact of water on reactor performance and the costs of ethanol feedstock and water removal from unconverted ethanol. Additional evaluation of the impact of water on catalyst deactivation should be performed as the latter is related to decay of process performance. Deactivation of one- and two-step catalysts by coking has been observed and coke precursors are believed to be bulky oxygenates from polycondensation of acetaldehyde [20,22,23,26,27,33,45,65]. In the two-step process, polycondensation of acetaldehyde can be hindered by operating at high ETOH/AC ratios [26] so that as soon as crotonaldehyde is formed it is reduced to crotyl alcohol with ethanol, preventing further aldol condensation reactions with other aldehydes. The addition of water to the feed might also result in a reduction of the formation of bulky oxygenates by water blocking of adjacent sites active for aldol condensation, as postulated for one-step catalysts [43], lowering the probability of successive aldol condensation reactions. This is a point yet to be studied.

Besides studying the effect of operating conditions, the presence of impurities in the reactant feed and catalyst deactivation, another important issue for efficiently designing a process is the availability of a kinetic model. There are few works on kinetic models, both for one- [47–49] and two-step [50,51] catalysts, probably because the reaction mechanism is complex, catalyst-dependent and difficult to unveil due to the instability of reaction intermediates. The latter, together with the formation of many side products, compel to make simplifications to tackle the problem. Only two works have been published on the kinetic modelling of two-step catalysts for the conversion of ethanol/acetaldehyde mixtures into 1,3-butadiene: Liu et al. [50] for a ZrO_2-MgO-SiO_2 catalyst and Dussol et al. [51] for a Ta_2O_5/SiO_2 catalyst. Liu et al. [50] considered the Toussaint-Kagan pathway for 1,3-butadiene formation while Dussol et al. [51] additionally considered the Inoue route, where acetone, a side product, is converted to methyl vinyl ketone (MVK), which is reduced to 3-buten-2-ol that finally dehydrates to 1,3-butadiene. While Dussol et al. [51] argued that the Inoue route explained 20–40% of butadiene formation, Liu et al. could successfully model 1,3-butadiene formation based only on the Toussaint-Kagan pathway, so it is unclear if the Inoue route is necessary for explaining 1,3-butadiene formation. Regarding side products, Liu et al. [50] described the formation of only the major ones, ethene and diethyl ether, resulting in a simplified reaction scheme, with only three reactions, that allowed them to use complex kinetic equations derived from proposed reaction mechanisms. On the other hand, Dussol et al. proposed a reaction scheme comprising 20 reactions, some of them reversible, to describe the formation of 1,3-butadiene and the many side products. Probably, because of the large number of reactions, they were compelled to use simpler kinetic equations than in the work by Liu et al., namely, power-law models. They made simplifications such as assuming the same kinetic parameters for those reactions that were similar in nature (e.g., dehydration, isomerization, etc.) and setting the value of the activation energy related to some minor products. Dussol et al. successfully modelled the main side products (ethene, diethyl ether) but failed to predict most of the minor products. A concern about these models is that they were not validated with experiments conducted with aqueous ethanol/acetaldehyde mixtures, which was the industrial practice, so it is not clear that they could be of use to design the reactor of the second reaction step of the Ostromislensky process.

The aim of this paper is to fill some gaps regarding the conversion of aqueous ethanol/acetaldehyde mixtures into 1,3-butadiene over two-step catalysts, with the aim to design more efficiently the industrial Ostromislensky process. For that purpose, the interaction between

operating conditions and water content in the conversion of aqueous ethanol/acetaldehyde mixtures over a two-step catalyst was studied by applying a design of experiments (DOE). A Ta-SBA-15 catalyst (~80% selectivity to butadiene) was chosen as a representative of new generation two-step catalysts [27]. A kinetic model which accounts for the presence of water in the feed is proposed and its kinetic parameters are estimated from the rate data generated in the DOE.

2. Materials and methods

2.1. Catalyst preparation and characterization

As commented above, a mesoporous Ta-SBA-15 catalyst reported by Chae et al. [27] was selected as it exhibits both high 1,3-butadiene selectivity and good coking tolerance. The catalyst, with a nominal Ta_2O_5 content of 2 wt%, was synthesized following the methodology reported in the work of Chae et al. [52]. More information on catalyst preparation can be found in the Supporting Information.

The catalyst properties were analyzed using different techniques, which are briefly mentioned here and in more detail in Appendix A of the Supporting Information. The content of Ta was measured by Inductively Coupled Plasma-Optical Emission Spectrometry (ICP-OES). The long-range ordering of the mesoporous channels in the calcined SBA-15 silica carrier and the Ta-SBA-15 catalyst was assessed by low-angle X-ray diffraction (XRD) and transmission electron microscopy (TEM). The presence of crystalline phases related to Ta (oxide) was evaluated by wide-angle XRD. Textural properties of the SBA-15 silica and the Ta-SBA-15 catalyst were determined by nitrogen physisorption. Diffuse reflectance UV–Vis spectroscopy was used to study the coordination of Ta atoms in the calcined Ta-SBA-15 sample. The density and strength of the Brønsted and Lewis acid sites in the Ta-SBA-15 catalyst were determined by FTIR spectroscopy of adsorbed pyridine at different desorption temperatures (150, 250, and 350 °C) [53].

2.2. Experimental facility and catalytic tests

Catalytic tests were carried out in a fixed bed continuous flow reactor operating at atmospheric pressure and using nitrogen as a carrier gas. Ethanol/acetaldehyde/water liquid mixtures were prepared and charged in a pressurized tank, and then fed into the reactor using a Bronkhorst® mini cori-flow [46]. Prior to the catalytic tests, the catalyst was pressed, crushed, and sieved to collect the 0.3–0.5 mm fraction. The internal diameter of the stainless-steel tube reactor was 0.83 cm and its length 25.8 cm. The bed was divided into three sections, separated by glass wool plugs. The top section was a SiC bed of 8 cm, the middle one comprised a bed of catalyst diluted in the necessary amount of SiC to obtain a bed length of 13 cm and the bottom section was also a SiC bed. The reactor was externally heated with an electric oven to control the reaction temperature. The reactor output line was electrically traced at 300 °C to avoid product condensation before analysis by on-line gas chromatography (GC) using an Agilent 7890A gas chromatograph. In the start-up, the catalyst was dried by preheating at 1 °C/min up to 400 °C while feeding 20 ml/min of nitrogen with a mass flow controller. After 1 h, the reactor was cooled down to the operating temperature at 1 °C/min and then liquid reactants were fed into the reactor. In all the experiments the partial pressure of ethanol in the reactor feed was fixed at 0.13 bar. For the experiments, the weight hourly space velocity (WHSV) was defined as the mass flow rate of ethanol and acetaldehyde (water-free) divided by the mass of catalyst in the reactor.

The simultaneous effect of temperature, ETOH/AC molar ratio, WHSV and water mass content in the ethanol feedstock was studied in a full factorial experiment, performing short-duration catalytic tests so that catalyst deactivation was negligible. For all combinations of three temperatures (300, 325, and 350 °C), two ETOH/AC molar ratios (1.7 and 2.7) and two water mass contents in the ethanol/acetaldehyde mixture (0 and 7.5% wt), four space velocities (WHSV of 0.22, 0.63, 1.12, and 1.63 h^{-1}) were assessed consecutively, from the largest to the lowest value, using a fresh load of catalyst. To check that catalyst deactivation was negligible, the first experiment was repeated at the end of the run of each temperature-ETOH/AC-water combination. Some additional tests were carried out for the anhydrous feed mixture at an ETOH/AC molar ratio of 2.2. The carbon balance error in all catalytic tests was usually below 10%, and only in some tests between 10 and 15%. Besides, to study the impact of water presence in the feed on catalyst deactivation, long-duration catalytic tests were performed. Catalyst stability was also studied by performing repeated cycles of operation-regeneration. Catalyst regeneration was carried out by raising the reactor temperature (1 °C/min ramp in a N_2 stream) until 500 °C and keeping this temperature under a flow of air of 40 ml/min for 8 h.

For all catalytic tests the reactant mixture was obtained by mixing the necessary amount of deionized Milli-Q water (in the case of the water-containing feedstock), anhydrous ethanol (Panreac, 99.8% *v*/v) and acetaldehyde (Sigma-Aldrich, purity ≥99.5%). When water was not added to the feed, the nitrogen flow was adjusted to keep the ethanol partial pressure constant. In the water-containing experiments, the necessary amount of nitrogen was replaced by water, therefore keeping constant the ethanol partial pressure and total volumetric flow for a given WHSV. Thus, WHSV is inversely related to contact time.

The rate data from the full factorial design of experiments are gathered in Tables S1 and S2 of the Supporting Information. Each experimental data point is the average of 3–5 measurements taken every 45 min. Total conversion, product carbon selectivity and 1,3-butadiene carbon yield were calculated as follows:

$$\text{Total conversion}\,(\%) = \text{TC} = \frac{[(F_{ETOH\_in} + F_{AC\_in}) - (F_{ETOH\_out} + F_{AC\_out})]}{(F_{ETOH\_in} + F_{Ac\_in})} \bullet 100$$

$$\text{Carbon selectivity to product k}\,(\%) = S_k = \frac{c_k \cdot F_{k\_out} \bullet 100}{2 \cdot [(F_{ETOH\_in} + F_{AC\_in}) - (F_{ETOH\_out} + F_{AC\_out})]}$$

$$\text{Butadiene carbon yield}\,(\%) = Y_{BD} = \frac{2 \cdot F_{BD\_out}}{(F_{EtOH\_in} + F_{Ac\_in})} \bullet 100$$

were F_k is the mole flow rate (mol/h) of compound k (ETOH for ethanol, AC for acetaldehyde and BD for 1,3-butadiene), being the subscript *in* for the reactor inlet and *out* for the outlet, and c_k the number of carbon atoms of compound k.

In the catalytic tests ethanol is fed in excess to the ethanol/acetaldehyde stoichiometric ratio (1:1), and thus, 1,3-butadiene yield is limited by acetaldehyde. Given an ethanol/acetaldehyde ratio in the feed, there exists a maximum 1,3-butadiene yield, defined as:

$$\text{Maximun } 1,3-\text{butadiene carbon yield } (\%) = Y_{BD}^{max} = \frac{2\cdot F_{AC\_in}}{(F_{ETOH\_in} + F_{AC\_in})} \bullet 100 = \frac{200}{(r+1)}$$

where r is the ETOH/AC mole ratio in the feed. The relative butadiene yield is defined as the ratio between the actual butadiene yield and the maximum butadiene yield:

$$\text{Relative } 1,3-\text{butadiene carbon yield } (\%) = Y_{BD}^{rel} = \frac{Y_{BD}}{Y_{BD}^{max}} \bullet 100$$

2.3. Kinetic model development

The methodology followed to develop a kinetic model of the Ta-SBA-15 catalyst that accounts for the presence of water in the feed is analogous to the one previously applied by the authors to a one-step catalyst [49]. Briefly, a simplified reaction scheme was proposed and for each reaction a power-law kinetics was assumed, featuring a corrective term to account for the inhibition or promotion of the reaction rate by water. Then, the parameters of the model were estimated by fitting a portion of the experimental data from the DOE. The rest of the experimental data was used to validate the kinetic model. Since in the DOE, short-duration catalytic tests were carried out so that catalyst deactivation was negligible, the proposed kinetics in this manuscript does not account for catalyst deactivation.

The numerous reactions occurring over the catalyst were simplified into a six-reaction scheme (reactions 1 to 6) that accounts for the formation of the main products (1,3-butadiene and water) as well as minor products (ethene, diethyl ether, alkenes, heavy compounds and other oxygenated compounds) observed in the catalytic tests. Since the catalyst lacks sites active for dehydrogenation, hydrogen was not observed in the reaction products, which was a constraint when considering the possible reactions comprising the reaction scheme.

$$C_2H_5OH + C_2H_4O \rightarrow C_4H_6 + 2H_2O \quad \text{(R1)}$$

$$C_2H_5OH \rightarrow C_2H_4 + 2H_2O \quad \text{(R2)}$$

$$2C_2H_5OH \rightarrow (C_2H_5)_2O + H_2O \quad \text{(R3)}$$

$$2C_2H_5OH \rightarrow C_4H_8 + 2H_2O \quad \text{(R4)}$$

$$C_2H_5OH + C_2H_4O \rightarrow C_4H_8O + H_2O \quad \text{(R5)}$$

$$3C_2H_4O \rightarrow C_6H_{12}O_3 \quad \text{(R6)}$$

The proposed reaction scheme does not represent the molecular mechanism over the catalyst surface, just the overall reactions from ethanol and acetaldehyde. In reaction 1, 1,3-butadiene is assumed to be formed from ethanol and acetaldehyde in accordance with the Toussant-Kagan pathway. This reaction is also compatible with alternative reaction pathways proposed in the literature, where 1,3-butadiene is formed from coadsorbed ethanol and acetaldehyde molecules [38,54,55]. Reactions 2 and 3 represent the formation of ethene and diethyl ether by ethanol dehydration, respectively. C_4 alkenes, namely, 1-butene, cis-2-butene, trans-2-butene and isobutene as well as 1-propene in a minor degree were observed in the reaction products. They all were lumped as alkenes and represented by 1-butene (C_4H_8). The formation of C_4 alkenes is believed to occur by dehydration of 1-butanol [49], formed by MPVO reduction of crotyl alcohol with ethanol [51]. Reaction 4, which represents formation of C_4 alkenes, is the aggregation of three reactions: crotyl alcohol formation from acetaldehyde and ethanol, 1-butanol formation from crotyl alcohol reduction with ethanol and 1-butanol dehydration to butenes. Many side reactions produced small amounts of numerous oxygenated compounds (ethyl acetate, acetone, butanal, 2-ethylbutanol, etc.). To simplify the modelling these compounds were lumped as oxygenated compounds, whose average molecular formula is close to that of butanal (C_4H_8O), and their formation represented by reaction 5. Finally, bulky oxygenates and aromatics were observed in the reaction products. These compounds, with more than six carbon atoms, were grouped and represented by paraldehyde, since its molecular formula is close to the average molecular formula of the heavy products. Since heavy products are believed to be initially formed by poly-condensation of acetaldehyde [56], reaction 6 was used to describe their formation in a simple manner. Ethanol might have a role in the formation of heavy compounds, but it must not be determining since the formation of heavy compounds is reasonable well predicted by the kinetic model with reaction 6, as it will be shown later.

A power-law kinetics was assumed for each reaction according to Eq. (1), where r_i is the reaction rate (mol/(g·h)) of reaction i, A_i is the rate constant at the reference temperature (T_{ref}=325 °C) in mol/(g ·h ·bar$^{\Sigma nki}$), Ea_i (kJ/mol) the activation energy, n_{ki} the reaction order of reactant k in reaction i, T the temperature in Kelvin and P_k (bar) the partial pressure of reactant k. All reactions were assumed irreversible. In the catalytic tests it was observed that the presence of water in the ethanol/acetaldehyde feed decreased the conversion of both ethanol and acetaldehyde. Therefore, an inhibition term $(1 + a_iP_{H2O})^{m_i}$ was introduced in the power-law kinetics, being a_i (bar^{-1}) and m_i fitting parameters and P_{H2O} the partial pressure of water along the reactor.

$$r_i = A_i e^{\left(\frac{-Ea_i}{R}\left(\frac{1}{T}-\frac{1}{T_{ref}}\right)\right)} \frac{\prod_{k=1}^{C} P_k^{n_{ki}}}{(1 + a_i P_{H_2O})^{m_i}} \quad i = 1....NR \quad (1)$$

In the kinetic model, the independent variables are the temperature and the reactant partial pressures while A_i, E_{ai}, n_{jk}, a_i and m_i are the parameters to be estimated (32 parameters). The parameters of the kinetic model were estimated by fitting the rate data from the DOE (Section 2.2). For this purpose, the principle of maximum likelihood was applied, which under some assumptions [57,59], is equivalent to minimizing the following objective function (Eq. (2)):

$$OF = \sum_{k=1}^{C} \sum_{j=1}^{N} \frac{\left(F_{kj} - \widehat{F}_{kj}\right)^2}{\sigma_{kj}^2} \quad (2)$$

where F_{kj} and $\widehat{F}_{kj}$ are the experimental and predicted mole flow rate, respectively, at the reactor outlet for compound (or lump) k in experiment j, σ_{kj} the standard deviation of the experimental error of the mole flow rate of the compound k in experiment j, N the number of experiments and C the number of compounds.

The predicted mole flow rates $\widehat{F}_{kj}$ were calculated by integrating the mole balance equations in the reactor (Eq. (3)):

$$\frac{d\widehat{F}_k}{dW} = \sum_{i=1}^{NR} \upsilon_{ki} r_i \qquad k = 1...C \quad (3)$$

where W is the mass of catalyst, υ_{ki} is the stoichiometric coefficient of compound k in reaction i and r_i the rate of reaction i. In Eq. (3) two simplifications were imposed: i) ideal plug flow (since both the axial Peclet number and the ratio between the length (L) and the diameter (D) of the catalyst bed were much greater than 1 [58]), and ii) internal and external mass transfer limitations were absent, and the controlling step was the chemical reaction. The latter was confirmed for every catalytic

test by studying the Mears criterion and the Weisz-Prater criterion for external and internal mass transfer limitation, respectively, as briefly summarized in Appendix D of the Supporting Information.

The experimental data from the catalytic tests were used to estimate the kinetic parameters and validate the kinetic model. From the 49 catalytic tests, 8 were rejected due to the large variability in the experimental results (see Section 3.2.2). Therefore, to validate the model 9 out of the remaining 41 catalytic tests were randomly set apart (validation data set) while the rest, 32 catalytic tests, was used to estimate the 32 parameters of the model (regression data set). Since C=9 and the regression data set comprises N=32 catalytic tests, the total number of experimental data points used in the fitting was 288, resulting in a ratio of 9 experimental data points per parameter to be estimated.

The algorithm to estimate the kinetic parameters is explained in detail in [49]. Here a brief description is provided. Starting from an initial guess of the kinetic parameters an iterative loop is performed whose first step is the search of kinetic parameters that minimize the objective function (Eq. (2)). This involves solving the mass balance equations in the reactor. To prevent overfitting due to the use of an excess number of parameters, the parameters estimated by the optimizer are statistically analyzed with hypothesis tests and the least significant parameter for a given confidence level is removed. The optimization is again performed, but with a reduced set of kinetic parameters. This loop is performed until all parameters retained in the model are significant. Once a final set of kinetic parameters is obtained, a confidence interval for each parameter is calculated.

3. Results and discussion

3.1. Physicochemical properties of SBA-15 silica and Ta-SBA-15 catalyst

The ordered mesoporous structure of the SBA-15 support and Ta-SBA-15 catalyst was confirmed by low-angle XRD, while the presence of Ta-related crystalline phases was assessed by wide-angle XRD in the 2θ range of 10°–90°. The low- and wide-angle XRD data are presented in Fig. S1a and S1b, respectively, of the Supporting Information. As observed in Fig. S1a, the low-angle XRD pattern of the pristine calcined SBA-15 silica carrier exhibits a main diffraction peak at 2θ of 0.93° with a shoulder at 1.3° related, respectively, to the (100,110) reflections characteristic of the hexagonal long-range ordering of tubular mesopores in this material. As also seen in Fig. S1a, no apparent changes in the pore structure of SBA-15 were noticed upon impregnation with the Ta precursor solution and subsequent calcination in air. The hexagonal arrangement of the unidirectional mesoporous channels in the Ta-SBA-15 catalyst was additionally confirmed by TEM (Fig. 1). Moreover, the

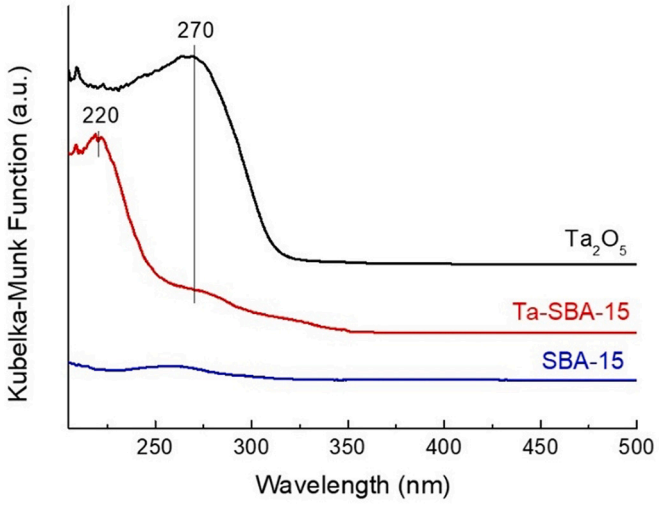

Fig. 2. Diffuse reflectance UV–Vis spectrum of calcined Ta-SBA-15. For comparison purposes, the spectra of the bare SBA-15 silica support and the reference Ta_2O_5 samples are also shown.

wide-angle XRD pattern of the calcined Ta-SBA-15 sample (Fig. S1b) did not exhibit reflections related to Ta_2O_5 crystallites, indicative of a high dispersion of the Ta species on the SBA-15 surface. Nevertheless, the presence of XRD-silent very small (< 3 nm) Ta_2O_5 crystallites and/or of a poorly crystallized Ta_2O_5 phase cannot be disregarded.

The nature of Ta species in the calcined Ta-SBA-15 catalyst was also studied by diffuse reflectance UV–Vis spectroscopy. The UV–Vis spectra of the pristine SBA-15 silica support, the Ta-SBA-15 catalyst, and the reference Ta_2O_5 sample are shown in Fig. 2. As observed, the SBA-15 silica did not exhibit any absorption, in agreement with previous reports [60]. Differently, the Ta-SBA-15 sample showed a main sharp absorption peak at ca. 220 nm, along with a much less intense and broader absorption feature with maximum at ca. 270 nm. The absorption at ca. 220 nm is ascribed to the oxygen-to-metal charge transition (CT) in isolated tetrahedral Ta(V) species (TaO_4) dispersed on silica [61]. Moreover, the weak and broad absorption feature at about 270 nm is related to hexacoordinated Ta(V) (TaO_6) in Ta_2O_5-like species [62], as supported by the presence of a broad absorption at about the same wavelength in the spectrum of the reference Ta_2O_5 sample (Fig. 2). The absence of reflections related to Ta_2O_5 nanoparticles in the wide-angle XRD pattern of Ta-SBA-15 (Fig. S1b) suggests that the minority Ta_2O_5-

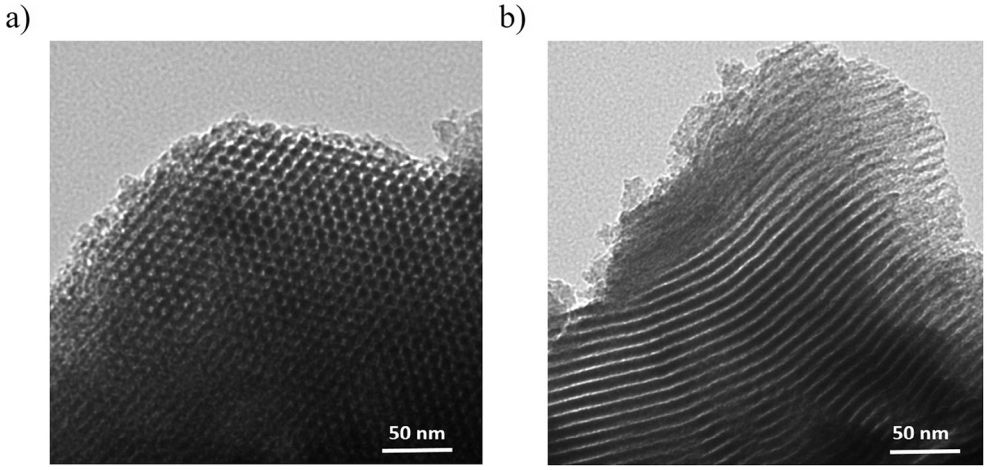

Fig. 1. Representative TEM images of the Ta-SBA-15 catalyst showing the long-range ordering of the hexagonally arranged mesopores viewed from a perpendicular (a) and parallel (b) perspective.

Table 1
Tantalum content (given as Ta_2O_5) and textural properties of calcined SBA-15 and Ta-SBA-15 samples.

Sample	Ta_2O_5 content[a] (wt%)	BET surface area (m^2/g)	Total pore volume (cm^3/g)	Average pore diameter (nm)
SBA-15	–	862	1.01	6.6
Ta-SBA-15	1.8	737	0.80	6.2

[a] Determined by ICP-OES.

like species detected by UV–Vis should have sizes below the XRD detection limit.

In conclusion, the characterizations by XRD and DR UV–Vis spectroscopy confirm the high dispersion of Ta species in the prepared Ta-SBA-15 catalyst, as also concluded for the equivalent sample reported in the work by Chae et al. [27], with a predominance of isolated Ta(V) species dispersed on the SBA-15 silica surface.

Both the calcined SBA-15 support and Ta-SBA-15 catalyst exhibited type IV N_2 adsorption isotherms with H1-type hysteresis loops at a relative pressure of 0.4–0.9 (Fig. S2a) due to capillary condensation within the mesopores, suggestive of a high uniformity in the size of mesopores. This is evidenced by the relatively narrow mono-modal pore size distributions (PSD) displayed by both samples, as shown in Fig. S2b, with pore diameters spanning from ca. 2 to 15 nm and maxima centered at 6.6 and 6.2 nm for SBA-15 and Ta-SBA-15, respectively. The slightly lower mean pore diameter obtained for Ta-SBA-15 is suggestive of the presence of Ta_2O_5 species highly dispersed within the mesoporous channel. The Ta content, as determined by ICP-OES, amounted to 1.8 wt % (given as Ta_2O_5), closely matching the nominal content of 2 wt% (Table 1), corresponding to a Ta/Si atomic ratio of 0.05. The textural properties of the bare SBA-15 silica and the Ta-SBA-15 catalyst are also given in Table 1. The high BET area (862 m^2/g) and total pore volume (1.01 cm^3/g) of the SBA-15 silica carrier sign for a high ordering of mesopores, in conformity with low-angle XRD and TEM. On the other hand, the Ta-SBA-15 catalyst presented a BET area of 737 m^2/g and a total pore volume (TPV) of 0.80 cm^3/g (Table 1), which represents a relative decrease of ca. 15% and 20% for BET area and TPV, respectively, with respect to the values of the bare SBA-15 support. This relatively small relative decrease in textural properties may be ascribed to a certain loss of long-range order in the arrangement of mesopores after impregnation of SBA-15 with the Ta precursor and subsequent calcination and probably also to a partial (minor) blockage of mesopores by in-pore highly dispersed Ta_2O_5 species.

Finally, the FTIR spectra of chemisorbed pyridine on Ta-SBA-15 recorded at desorption temperatures of 150, 250, and 350 °C are presented in Fig. 3. As observed, a very weak band at ca. 1545 cm^{-1} associated to protonated pyridine (PyH^+) is perceived at a desorption temperature of 150 °C, hinting to the existence of a minor amount of Brønsted acid sites (BAS) on the surface of Ta-SBA-15. The fact that the IR band at 1545 cm^{-1} is virtually absent at higher pyridine desorption temperatures (Fig. 3) evidences that the BAS are rather weak in nature. The presence of a few weak BAS in Ta-containing SBA-15 silica materials has been attributed to some silanol groups whose acid strength is enhanced by the interaction with nearby Ta(V)-related Lewis acid sites (LAS) [60]. Indeed, the relatively intense band at ~1450 cm^{-1} confirms the existence of a comparatively high amount of LAS associated to Ta^{5+} species in our Ta-SBA-15 catalyst (Fig. 3), as it was also found for similar silica-supported Ta catalysts [60,63,64]. At a desorption temperature of 150 °C, the density of LAS amounted to 39 μmol/g, and was remarkably reduced to 13 μmol/g upon increasing the temperature to 250 °C. However, a further raise in temperature to 350 °C produced only a minor decrease in the concentration of LAS from 13 to 10 μmol/g. Therefore, according to FTIR-pyridine measurements, the Ta-SBA-15 catalyst contains essentially Lewis-type acid sites, of which about 25% exhibit a relatively high acid strength, capable of retaining pyridine after desorption at 350 °C.

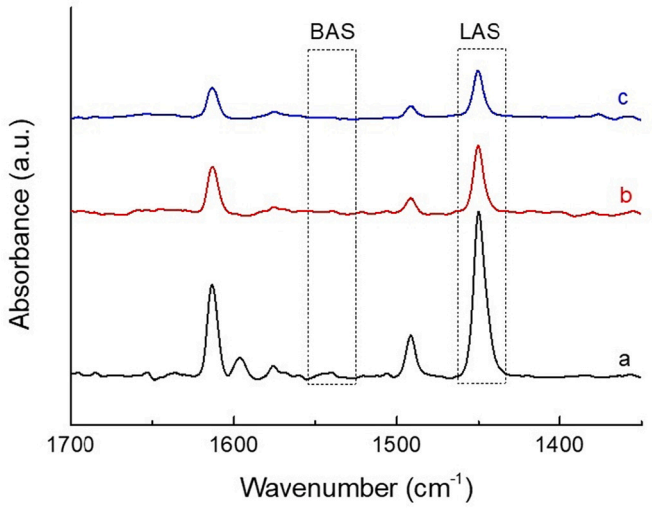

Fig. 3. FTIR-pyridine spectra for sample Ta-SBA-15 recorded at desorption temperatures of 150 °C (a), 250 °C (b), and 350 °C (c). BAS and LAS stand for Brønsted and Lewis acid sites, respectively.

3.2. Effect of reaction conditions

3.2.1. Temperature, space velocity and ethanol/acetaldehyde molar ratio

First, the combined effect of reaction temperature, WHSV, and ethanol/acetaldehyde molar ratio on the catalyst performance is discussed based on the experiments carried out with anhydrous ethanol/acetaldehyde feeds. Since it was observed that temperature and space velocity had the same qualitative effect on total conversion and selectivity to products at ETOH/AC=1.7 than at 2.7, only the results at ETOH/AC=1.7 are discussed next.

Fig. 4 shows the combined effect of temperature and space velocity on total conversion, 1,3-butadiene yield and selectivity for the catalytic tests carried out at ETOH/AC=1.7. As shown in Fig. 4a, total conversion decreases almost linearly with space velocity, regardless of temperature, in the range of studied space velocity, while increases nonlinearly with temperature. The same trends are observed for 1,3-butadiene yield (Fig. 4b), in agreement with [37]. On the other hand, the sensitivity of 1,3-butadiene selectivity to space velocity significantly depends on the operating temperature (Fig. 4c): it can be small (325 °C), as reported by Han et al. [34] and Xu et al. [32], exhibits a maximum (300 °C), as reported by Yang et al. [25], or rapidly decline at low space velocity (350 °C). The reason of the small effect of WHSV on 1,3-butadiene selectivity at 325 °C with the Ta-SBA-15 catalyst is that the decrease in selectivity to ethene, diethyl ether and alkenes with WHSV is almost counterbalanced by the increase in selectivity to oxygenates (Table S1, tests 14–17). At 350 °C, the rapid decrease in 1,3-butadiene selectivity at low space velocity (Fig. 4c) is because at high conversion, most of acetaldehyde has been consumed near the outlet of the reactor, and the excess of ethanol tends to dehydrate rather than to be converted to 1,3-butadiene since ethanol dehydration prevails [25,32]. This result points out that ethanol dehydration reactions (reactions 2 and 3) have higher apparent activation energies than the 1,3-butadiene formation reaction (reaction 1), which is confirmed later (Section 3.4, Table 2). While the selectivity to ethene and diethyl ether increases with temperature

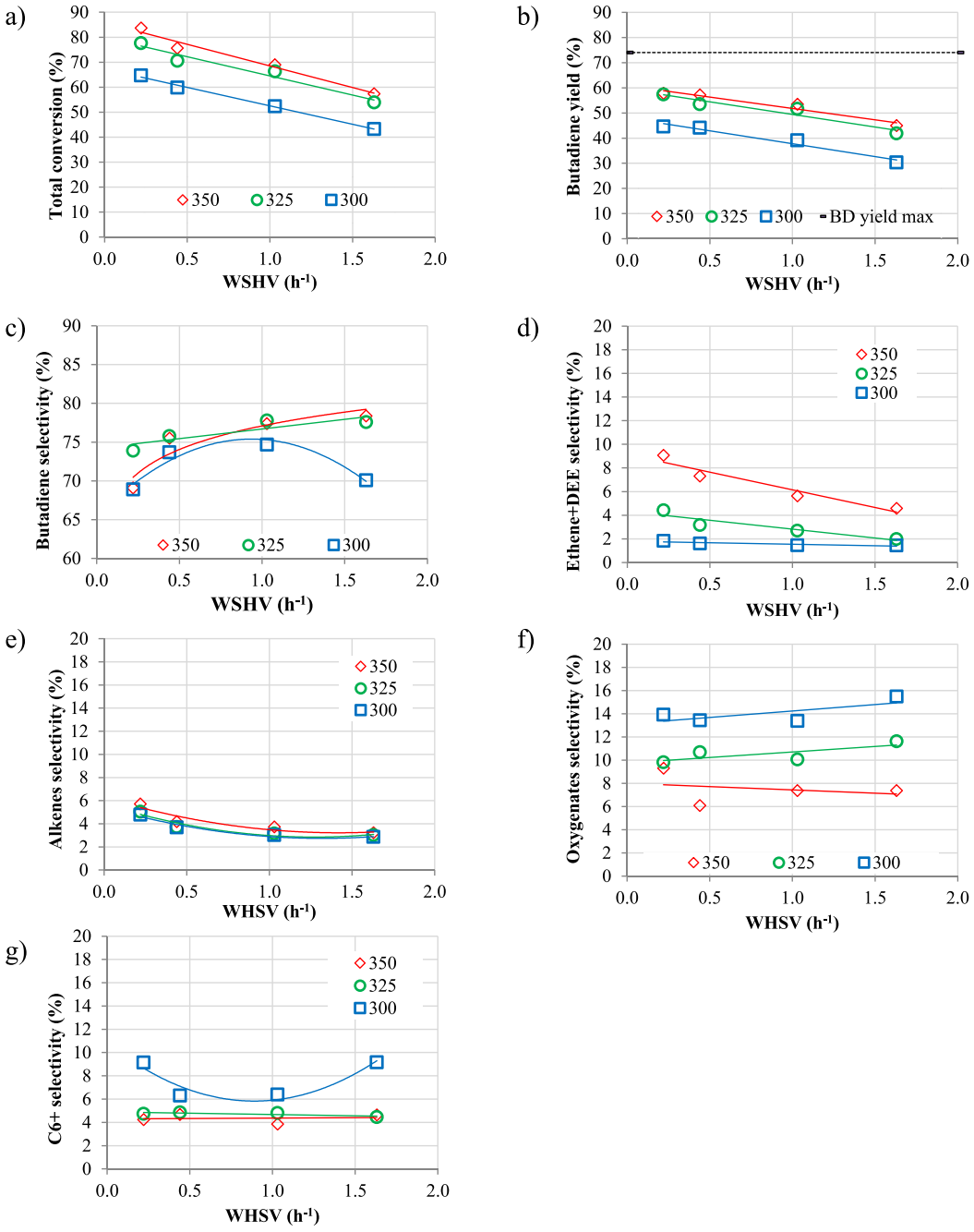

Fig. 4. Effect of space velocity (WHSV) and temperature on total conversion, 1,3-butadiene yield and selectivity to products. Operating conditions: anhydrous feed with ethanol/acetaldehyde molar ratio of 1.7.

(Fig. 4d), the opposite is observed for light oxygenates and heavy compounds (C_{6+}) (Fig. 4f and g). A possible explanation for the latter is that, as temperature rises, both acetaldehyde aldol-condensation to crotonaldehyde and MVPO reduction of crotonaldehyde are enhanced, thereby increasing 1,3-butadiene formation, and avoiding side reactions of acetaldehyde to oxygenates and self- and cross-condensation of crotonaldehyde to heavy compounds, respectively. This interpretation is compatible with the fact that the apparent activation energy of 1,3-butadiene formation (reaction 1) is greater than that of oxygenates (reaction 5) and heavy compounds (reaction 6), as it will be shown later in Section 3.4 (Table 2). It is somewhat surprising that the formation of heavy compounds decreases with temperature given that the very opposite was observed in our previous work with a one-step catalyst [43]. A plausible reason is that over a two-step catalyst there is a relative excess of ethanol, that increases as acetaldehyde is converted, thereby favoring the MPVO reaction of crotonaldehyde over its conversion to heavy compounds. However, over a one-step catalyst the reaction mixture is depleted of ethanol as the reaction proceeds, so there is less ethanol available to reduce crotonaldehyde as it is formed, which increases the probability of its conversion to heavy compounds with temperature.

For a fixed temperature and space velocity (Fig. 5), 1,3-butadiene yield decreases in absolute terms with the ETOH/AC ratio, but it increases relative to the maximum 1,3-butadiene yield achievable, since the MPVO reduction of crotonaldehyde is promoted by the larger amount of ethanol in excess. A drawback of operating with a large ETOH/AC feed ratio is that more ethanol can be converted through

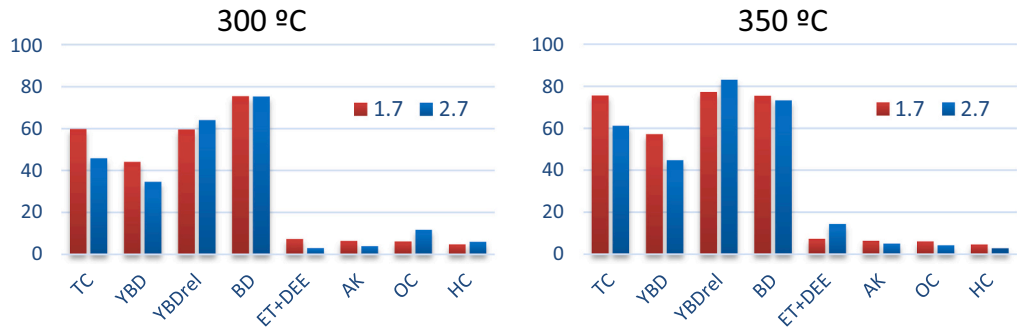

Fig. 5. Effect of ethanol/acetaldehyde molar ratio (1.7 and 2.7) and temperature (Left: 300 °C, Right: 350 °C) at WHSV = 0.44 h^{-1}on total conversion (TC), absolute (Y_{BD}) and relative (Y_{BD}^{rel}) 1,3-butadiene yield and selectivity to products (BD = 1,3-butadiene; ET: ethene; DEE: diethyl ether; AK: alkenes; OC: oxygenated compounds; HC: heavy compounds).

secondary reactions. At low temperature (300 °C), selectivity to oxygenates significantly increases with ETOH/AC ratio (Fig. 5-left), while at high operating temperature (350 °C), where dehydration of ethanol is promoted, selectivity to ethene and diethyl increases in detriment of 1,3-butadiene selectivity (Fig. 5-right) [28,32]. From a process point of view, the operation at larger ETOH/AC ratios in the reactor feed involves a larger ethanol recycle, which translates into higher operating and investment costs for the separation and recycle of ethanol. Therefore, the ETOH/AC ratio is a key operating variable and should be carefully selected to economically optimize the plant.

3.2.2. *Effect of water content in the ethanol/acetaldehyde mixture*

For the sake of simplicity, only the results obtained at ETOH/AC = 1.7 are discussed next, since the observed effects of water at ETOH/AC = 2.7 are qualitatively similar. Regarding temperature, the discussion is only based on the catalytic tests performed at 325 °C and 350 °C. The results of the catalytic tests at 300 °C with aqueous ethanol/acetaldehyde mixtures were disregarded since a large variability in the catalyst performance was observed in these tests, preventing any reliable conclusion.

As shown in Fig. 6a, at 325 °C the presence of water in the feed decreases total conversion, particularly at high WHSV. At high temperature (350 °C, Fig. 6b), this effect is not clearly observed at any WHSV, since the difference in conversion between anhydrous and aqueous feeds is small. At any temperature, water in the feed barely affects catalyst selectivity as inferred from the similar yield to any product at a given total conversion for anhydrous and aqueous feeds, as exemplified in Fig. 6c and 6d (1,3-butadiene), 6e and 6f (ethanol dehydration products) and 6g and 6h (heavy compounds). Therefore, a decrease in the yield of 1,3-butadiene by the presence of water in the feed could be just counteracted by either reducing the space velocity, keeping constant the operating temperature, or increasing the operating temperature, keeping constant the space velocity.

The presence of water in the feed in the ethanol-to-1,3-butadiene reaction over one-step metal-doped silica-supported catalysts produced some effects that are worthy of mention here. On the one hand, it undesirably increased the selectivity to ethene and diethyl ether, due to the water-induced transformation of Lewis acid sites to Brønsted acid sites [38,40,43], and also inhibited the formation of heavy compounds [43], due to the blocking by water of the Lewis acid sites active for aldol condensation. However, none of these effects were observed for the two-step Ta-SBA-15 catalyst. The fact that the selectivity to ethene and diethyl ether is hardly modified by the presence of water in the feed might be tentatively ascribed to a lack of generation of Brønsted acid sites in the Ta-SBA-15 catalyst or, if formed, their acidity is too weak to effectively catalyze the dehydration reactions at the studied reaction conditions. The impact of water on heavy compound formation is difficult to assess since the yield of heavy compounds is already small for the anhydrous feed. In any case, it seems plausible that water is adsorbed on the active Ta(V) Lewis acid sites of the catalyst, particularly at the lower temperature (325 °C), resulting in the observed decrease in ethanol and acetaldehyde conversion, and therefore, in 1,3-butadiene yield. At higher temperature (350 °C), water adsorption would be more hindered, which would explain why catalyst performance barely changes when shifting from an anhydrous to a hydrous ethanol/acetaldehyde feed, at least, for the studied range of water content in the feed.

3.3. *Long-term stability and regeneration of the catalyst*

Long catalytic tests were carried out with the Ta-SBA-15 catalyst to analyze its deactivation and regeneration as well as to assess the impact of the presence of water in the feed on its stability with time-on-stream. A first test was performed with an anhydrous feed and a relatively fast initial deactivation of the catalyst was observed, decreasing the conversion around 15 percentage points during the first 25 h of reaction (Fig. 7). During the test, the product distribution barely changed, which is characteristic of two-step catalysts [19], and only a slight decline was observed in the selectivity to 1,3-butadiene and ethanol dehydration products in favor of heavy compounds. As shown in Fig. 7, the catalyst fully recovered its activity after regeneration by calcination in air at 500 °C for 8 h, which is suggestive of coke deposition as the main reason for its deactivation [65].

Another test with a fresh catalyst load was carried at the same temperature and ETOH/AC ratio, but with the presence of water in the feed (7.5 wt%) (Fig. 8). The space velocity was modified so the initial total conversion was close to that of the previous test with the anhydrous feed. The initial conversion decreased around 15 percentage points in 140 h, i.e., the rate of deactivation was 5.5 times lower than when water was not present in the feed. As a reference, only a small decrease in the deactivation rate of the industrial Ta_2O_5/SiO_2 catalyst was observed when increasing the water content in the ethanol/acetaldehyde feed [26]. Again, the Ta-SBA-15 catalyst fully recovered its initial activity upon regeneration by calcination in air at 500 °C. Presumably, catalyst deactivation is caused by very heavy compounds, which deposit on the catalyst surface, blocking the access of reactants to the active sites of the catalyst. The yield of heavy compounds is almost unaffected by the presence of water in the feed (Section 3.2.2) and thus, in principle, the rate of deactivation should not vary remarkably. A possible reason is that what changes is the nature of the coke rather than the total amount of coke, as observed by Zhang et al. over a $ZnO/ZrO_2/SiO_2$ catalyst when adding water (10 vol%) to an ethanol/acetaldehyde feed [65]. To find the exact reasons for this remarkable increase in catalyst stability by water requires a thorough study which is out of the scope of the present study and will be addressed in a future work.

3.4. *Kinetic model*

The estimated kinetic parameters are shown in Table 2 while Fig. 9

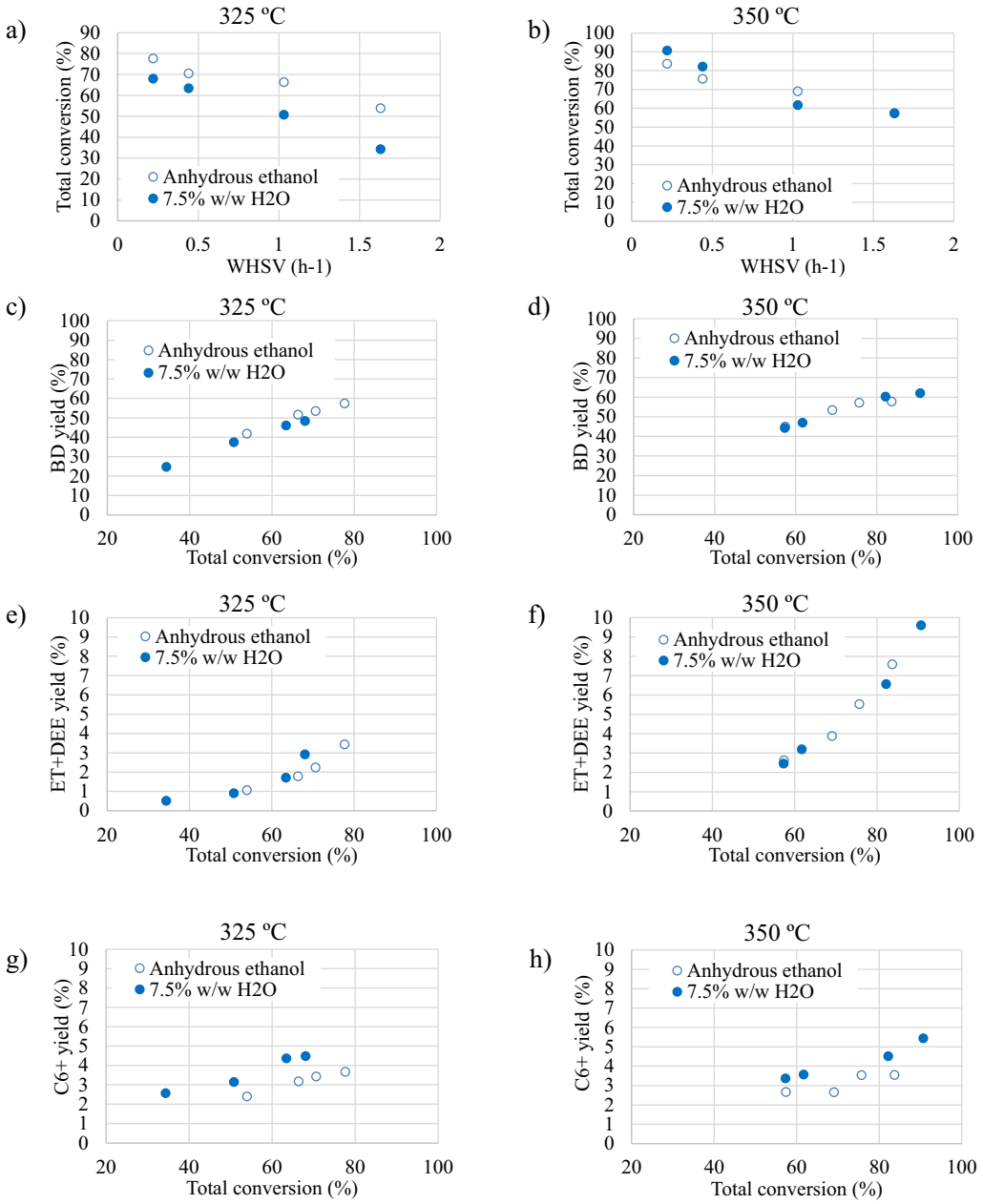

Fig. 6. Effect of water content (0 and 7.5 wt%) in the ethanol/acetaldehyde feed on total conversion (a-b) and yield to products (c-h) at 325 °C (left panels) and 350 °C (right panels).

shows the experimental mole flow rates in the regression data set against those predicted by the model for each compound/lump. Model predictions are good not only for all the major compounds/lumps at the reactor outlet (ethanol, acetaldehyde, 1,3-butadiene, water, oxygenated compounds and ethene) but also for the lump of heavy compounds. The latter is noteworthy since heavy compounds are a minor fraction of the reaction products and only one reaction has been used to predict an aggregation of multiple compounds that are formed through different reactions. Regarding diethyl ether and alkenes, which are minor compounds/lumps, the fitting is acceptable for diethyl ether, but it is poor for the alkenes, being overpredicted when the formation of alkenes is relatively low and underpredicted when the formation of alkenes is relatively high. Thus, reaction and product lumping for the alkenes does not produce as good results as for the other lumps but, being a minor fraction of the reaction products, it is not a critical issue. Overall, more than 90% of the data points lie within the ±20% error bands so this result indicates that the chosen reaction scheme includes the most important reactions occurring over the catalyst.

The assumptions considered for the regression of the model, that the errors follow a normal distribution and have a constant variance, were validated through the analysis of the residuals [66]. The standardized residuals (Fig. S3) fairly follow a normal distribution, so the normality hypothesis is validated. When plotted against the predicted values, they also do not follow any trend and no significant change is observed in their spread around the zero line as one moves from left to right along the plots (Fig. S4), validating the constant variance hypothesis. The generalization capability of the kinetic model was assessed by comparing its predictions against the validation data set (Fig. S5). The generalization capability of the model is good since again more than 90% of the predictions lie within the 20% error bands. As expected, only for the alkenes, the prediction is somewhat poor. Therefore, the kinetic model can be a useful tool in the design of an industrial process of the

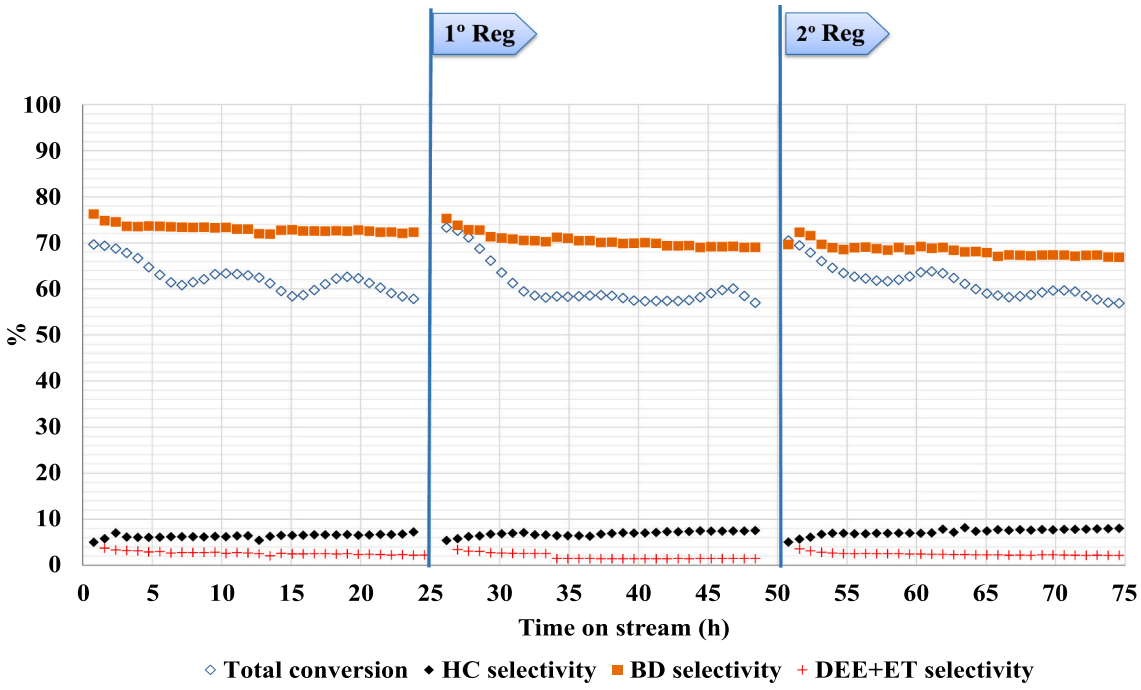

Fig. 7. Ethanol and acetaldehyde conversion and selectivity to main products with time-on-stream when water is not present in the feed. Operating conditions: WHSV = 1.03 h^{-1}, T = 325 °C, ETOH/AC = 1.7, P_{ETOH} of 0.13 bar and total pressure of 1 bar. Regenerations were carried out at 500 °C for 8 h under flowing air (30 ml/min).

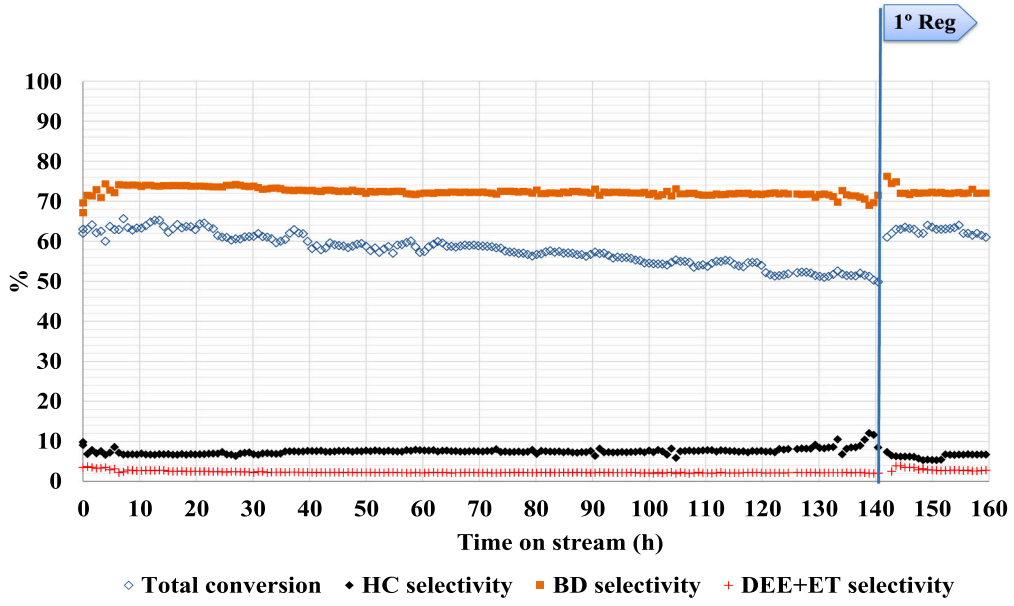

Fig. 8. Ethanol and acetaldehyde conversion and selectivity to main products with time-on-stream when water is present in the feed. Operating conditions: 7.5 wt% of water in the feed, WHSV = 0.73 h^{-1}, T = 325 °C, ETOH/AC = 1.7, P_{ETOH} = 0.13 bar and total pressure of 1 bar. Regenerations were carried out at 500 °C with air flow of 30 ml/min for 8 h.

Table 2
Estimates of the kinetic parameters.

Reaction	A (mol/g· h ·$bar^{\Sigma nki}$)	Ea (kJ/mol)	Reaction order ETOH	Reaction order AC	a (bar^{-1})	m
r_1	6.17 ± 0.12	53.33 ± 0.11	0.85 ± 0.31	1.41 ± 0.01	4.54 ± 0.16	1.99 ± 0.05
r_2	(9 ± 2)·10^{-3}	164.58 ± 2.85	1.54 ± 0.01	–	n.s	n.s
r_3	(27 ± 2)·10^{-3}	87.22 ± 0.61	2.50 ± 0.07	–	n.s	n.s
r_4	(3 ± 0.6)·10^{-3}	46.10 ± 1.89	1.10 ± 0.03	–	n.s	n.s
r_5	5.23 ± 1.01	20.00 ± 0.47	1.51 ± 0.08	1.67 ± 0.02	n.s	n.s
r_6	(56 ± 2) ·10^{-3}	22.00 ± 0.31	–	1.65 ± 0.01	n.s	n.s

n.s: found non-statistically significant.

two-step conversion of ethanol to 1,3-butadiene by allowing to assess the impact on process performance of the reaction conditions in the second reaction stage and the use of aqueous ethanol as feedstock.

The capability of the model to deal with aqueous ethanol/acetaldehyde feeds relies on the water corrective terms introduced in the power-law kinetics. Only the water corrective term of the 1,3-butadiene formation reaction (reaction 1) was found statistically significant. The reason is that the presence of water in the feed can substantially decrease

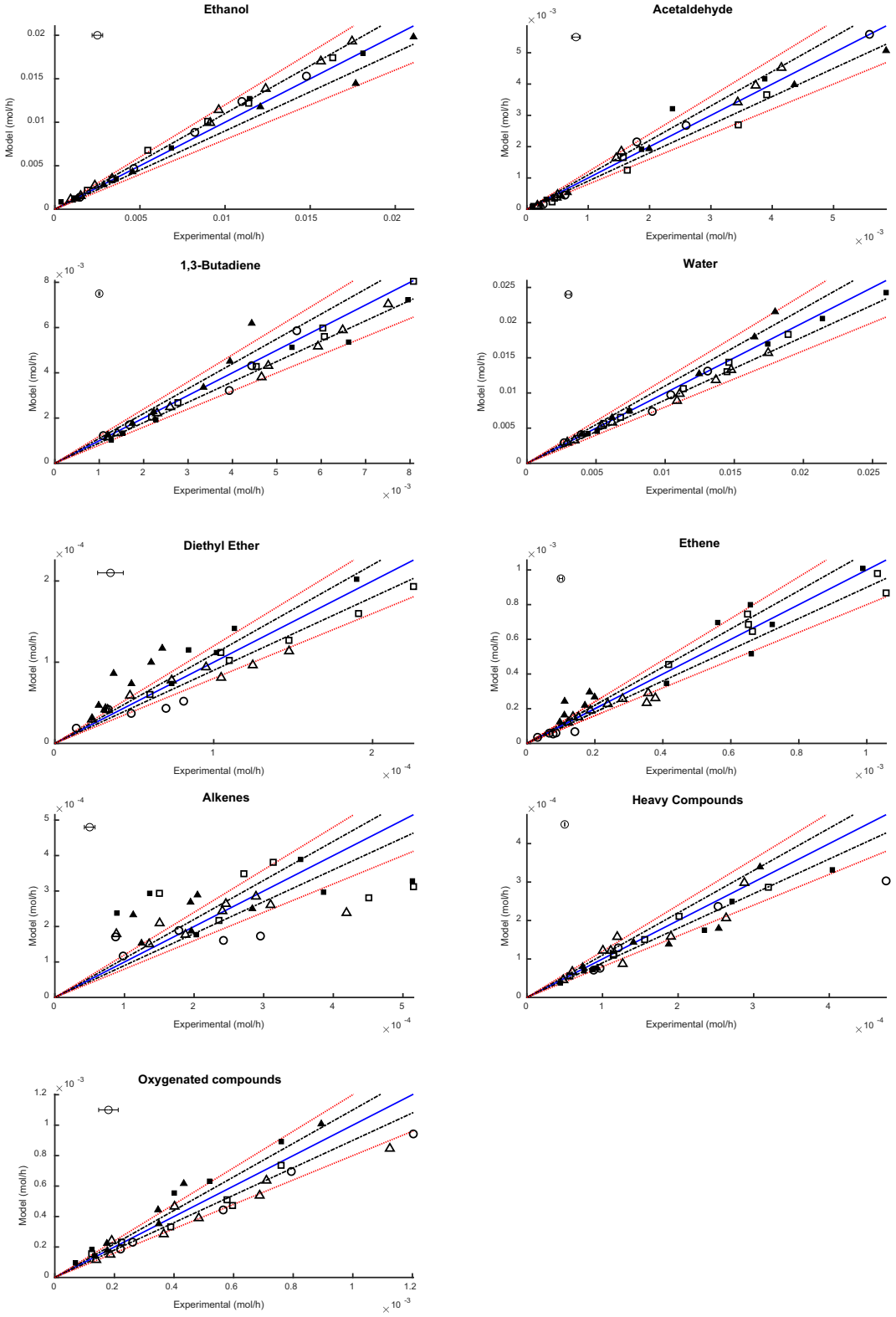

Fig. 9. Parity plots for the experimental and predicted mole flow rates for each compound/lump. (Temperature of catalytic tests: ● 300 °C, ▲325 °C and ■ 350 °C; Water content in feed shown with marker colour: white 0 wt%, black 7.5 wt%); Error bands: 10% (black dash-dotted line), 20% (red dotted line). For each chemical species, the average uncertainty of the experimental mole flow rates is shown in the upper-left side of the plot.

ethanol and acetaldehyde conversion, and therefore, the yield to all reaction products, but only the yield to 1,3-butadiene is significantly affected since the yield to the other reaction products is much lower, and their absolute change is insignificant relative to that of 1,3-butadiene. Thus, the use of a water corrective term for the minor reaction products does not statistically improve the predictions of the model for these compounds.

A brief comparison with the only two kinetic models of two-step catalysts published in the literature [50,51], which were commented in the introduction section, is presented next. It is remarked that those kinetic models were not validated with experiments conducted with aqueous ethanol/acetaldehyde mixtures, so their prediction capability in that case is unknown. Regarding the reaction scheme, Dussol et al. [51] claimed that, besides the Toussant-Kagan pathway, a new reaction pathway, the so-called Inoue route, should be considered in the reaction scheme for explaining 20–40% of 1,3-butadiene formation. We believe that the Inoue route is superfluous, given the similarity of the catalysts used on both works (tantalum oxide over silica) and that we have been able to model 1,3-butadiene formation only based on the Toussant-Kagan pathway, like Liu et al. [50] did for a ZrO_2-MgO-SiO_2 catalyst.

A comparison of the kinetic parameters between the kinetic models is difficult, given the different modelling approaches, catalytic systems, and reaction schemes. Hence, only the (apparent) activation energies estimated in the different works for the most important reactions are compared. The estimated activation energies for the 1,3-butadiene formation reaction are very close, ranging 40–55 kJ/mol. Also, very similar activation energy of the ethanol dehydration reaction to ethene is reported by Dussol et al. (157 kJ/mol) and this work (~165 kJ/mol), but they highly differ with that reported by Liu et al. (~41 kJ/mol). The situation is similar for the dehydration reaction of ethanol to diethyl ether (Dussol et al.: 103 kJ/mol; this work: ~83 kJ/mol; Liu et al.: ~20 kJ/mol). The similarity in these activation energies between this work and that by Dussol et al. might be due to the use of the same catalytic system. Experimental evidence shows that over one- and two-step catalysts ethanol dehydration reactions are more favored with temperature than 1,3-butadiene formation [19], so for the ethanol dehydration reactions larger activation energies than that of 1,3-butadiene formation reaction would be expected, which is not the case for the work by Liu et al. These incongruences show the need of more kinetic studies of two-step catalysts, particularly using aqueous feeds, to alleviate the scarcity of works on this subject.

4. Conclusions

The design of industrial processes to produce 1,3-butadiene from ethanol, based on the recent development of a new generation of catalysts, needs the study of important practical aspects: i) the effect of operating conditions and the presence of impurities (water) in the ethanol feedstock on the catalyst performance; ii) stability and regeneration of the catalysts and, iii) the development of kinetic models that can be used as a tool for designing the industrial process. These three key aspects have been addressed in this work for the second reaction stage of a two-step ethanol-to-butadiene process, where a mesoporous Ta-SBA-15 catalyst was chosen as a representative of the new generation of two-step catalysts.

The results showed that there are large non-linear interacting effects between the reaction conditions (temperature, space velocity and ethanol/acetaldehyde mole ratio) which must be carefully selected to optimize the catalyst performance. The effect of shifting from an anhydrous to an aqueous (7.5 wt%) ethanol/acetaldehyde feed was also studied since it allows to assess the option of using cheaper azeotropic ethanol feedstock instead of anhydrous grade ethanol. At high temperature, catalyst performance was barely affected by water in the feed while at low temperature ethanol and acetaldehyde conversion decreased, and consequently, also the 1,3-butadiene yield. A plausible explanation is that at low temperature water is strongly adsorbed on the Ta(V) Lewis acid sites of the catalyst, where formation of 1,3-butadiene occurs, but as temperature increases, the adsorption competition of water with reactants is hindered to the point that catalyst performance is almost unaffected by water in the feed. The nature of the active sites of the catalyst was not changed by water in the feed since, for a given total conversion of ethanol and acetaldehyde, selectivity to products for the aqueous and anhydrous feed were almost identical. This is an important difference with one-step catalysts, whose selectivity to ethanol dehydration products increases due to the transformation of some of their Lewis acid sites to Brønsted acid sites by water in the feed [38,40,43]. It was also found that water in the feed increased the stability of Ta-SBA-15 catalyst, reducing by 5.5-fold the deactivation rate compared to the case of an anhydrous feed, an effect that was also observed for one-step catalysts [43].

A kinetic model for the conversion of ethanol/acetaldehyde mixtures over the Ta-SBA-15 was developed, whose novelty lies in the use of kinetic equations that account for the effect of water in the feed on the catalyst performance. The model comprised six reactions, six chemical species and three lumps to account for the formation of the main and minor reaction products formed over two-step catalysts. Experimental data from the catalytic tests where the effect of water in the feed and reaction conditions was assessed on the performance of the Ta-SBA-15 catalyst were used for the regression and validation of the kinetic model. The results showed that the model can predict well the effect of reaction conditions and water content in the feed on the formation of major and most minor compounds. The modelling approach to build the kinetic model is expected to be valid for any other two-step catalyst. Future work will deal with further development of the kinetic model to account for catalyst deactivation. This requires conducting long-term experiments at different reaction conditions to extract information on catalyst deactivation and introduce corrective terms in the rate equations that account for the decay of catalyst activity.

Nomenclature

A	kinetic constant at reference temperature (mol/g h $bar^{\Sigma ni}$)
a	model parameter of water corrective term
AC	acetaldehyde
AK	alkenes
BD	1,3-butadiene
C	total number of compounds
c	number of carbon atoms
D	reactor diameter
DEE	diethyl ether
ET	ethene
e	residual
Ea	activation energy (kJ/mol)
ETOH	ethanol
F_k	mole flow rate of compound k (mol/h)
FTIR	Fourier-transform infrared spectroscopy
HC	heavy compounds
L	reactor length
m	exponent of the water corrective term
n	reaction order or number of carbon atoms
N	total number of tests
NR	number of reactions in the kinetic model
OC	oxygenated compounds
OF	objective function
P	total pressure (bar)
P_k	partial pressure of compound k (bar)
r	reaction rate (mol/h g)
R	ideal gas constant (8.314 J/mol K)
S	carbon selectivity
T	reaction temperature (°C or K)
TC	total conversion
W	mass of catalyst (g)

Wc	water mass content in ethanol feed (wt%)
WHSV	weight hourly space velocity (h^{-1})
XRD	X-ray powder diffraction
Y	carbon yield

Subscripts/Superscript

i	reactions
in	reactor inlet
j	experiments
k	compounds
max	maximum theoretical carbon yield
out	reactor outlet
rel	relative to maximum theoretical carbon yield

Greek letters

σ	standard deviation
υ	stoichiometric coefficient

Funding information

This work was carried out in the framework of the project "Bio-butadiene production from bioethanol" (CTQ2015-71427-R), which is funded by the Spanish Ministry of Economy, Industry and Competitiveness (MINECO) through the European Regional Development Fund (ERDF).

Declaration of Competing Interest

The authors declare that they have no known competing financial interests or personal relationships that could have appeared to influence the work reported in this paper.

Appendix A. Supplementary data

Supplementary data to this article can be found online at https://doi.org/10.1016/j.fuproc.2021.107092.

References

[1] European Commission, Going Climate-Neutral by 2050, Facilities, 2018.
[2] European Commission, A clean planet for all, in: A European Strategic Long-Term Vision for a Prosperous, Modern, Competitive and Climate Neutral Economy, 2018. COM(2018) 773 final.
[3] J.S.P.S. Irvin L. Murray, Jay L. Marsh, Process for Making Butadiene, US2403742, 1946.
[4] A. Talalay, L. Talalay, S.K.-The Russian synthetic rubber from alcohol - A survey of the chemistry and technology of the lebedev process for producing sodium-butadiene polymers, Rubber Chem. Technol. 15 (1942) 403–429. http://rubberchemtechnol.org/doi/pdf/10.5254/1.3543128.
[5] G. Giannakakis, A. Trimpalis, J. Shan, Z. Qi, S. Cao, J. Liu, J. Ye, J. Biener, M. Flytzani-Stephanopoulos, NiAu single atom alloys for the non-oxidative dehydrogenation of ethanol to acetaldehyde and hydrogen, Top. Catal. 61 (2018) 475–486, https://doi.org/10.1007/s11244-017-0883-0.
[6] J. Shan, J. Liu, M. Li, S. Lustig, S. Lee, M. Flytzani-Stephanopoulos, NiCu single atom alloys catalyze the C–H bond activation in the selective non- oxidative ethanol dehydrogenation reaction, Appl. Catal. B Environ. 226 (2018) 534–543, https://doi.org/10.1016/j.apcatb.2017.12.059.
[7] J. Shan, N. Janvelyan, H. Li, J. Liu, T.M. Egle, J. Ye, M.M. Biener, J. Biener, C. M. Friend, M. Flytzani-Stephanopoulos, Selective non-oxidative dehydrogenation of ethanol to acetaldehyde and hydrogen on highly dilute NiCu alloys, Appl. Catal. B Environ. 205 (2017) 541–550, https://doi.org/10.1016/j.apcatb.2016.12.045.
[8] G. Garbarino, P. Riani, M. Villa García, E. Finocchio, V. Sanchez Escribano, G. Busca, A study of ethanol dehydrogenation to acetaldehyde over copper/zinc aluminate catalysts, Catal. Today (2019) 0–1, https://doi.org/10.1016/j.cattod.2019.01.002.
[9] I.S.P. Campisano, C.B. Rodella, Z.S.B. Sousa, C.A. Henriques, V. Teixeira da Silva, Influence of thermal treatment conditions on the characteristics of Cu-based metal oxides derived from hydrotalcite-like compounds and their performance in bio-ethanol dehydrogenation to acetaldehyde, Catal. Today 306 (2018) 111–120, https://doi.org/10.1016/j.cattod.2017.03.017.
[10] I.C. Freitas, S. Damyanova, D.C. Oliveira, C.M.P. Marques, J.M.C. Bueno, Effect of Cu content on the surface and catalytic properties of Cu/ZrO2catalyst for ethanol dehydrogenation, J. Mol. Catal. A Chem. 381 (2014) 26–37, https://doi.org/10.1016/j.molcata.2013.09.038.
[11] G. Carotenuto, R. Tesser, M. Di Serio, E. Santacesaria, Bioethanol as feedstock for chemicals such as acetaldehyde, ethyl acetate and pure hydrogen, Biomass Convers. Biorefinery. 3 (2013) 55–67, https://doi.org/10.1007/s13399-012-0045-3.
[12] S. Bhattacharyya, Kinetic study on the mechanism of the catalytic conversion of ethanol to butadiene, J. Catal. 7 (1967) 152–158, https://doi.org/10.1016/0021-9517(67)90053-X.
[13] M. Gao, Z. Liu, M. Zhang, L. Tong, Study on the mechanism of butadiene formation from ethanol, Catal. Lett. 144 (2014) 2071–2079, https://doi.org/10.1007/s10562-014-1370-x.
[14] W. Janssens, E.V. Makshina, P. Vanelderen, F. De Clippel, K. Houthoofd, S. Kerkhofs, J.A. Martens, P.A. Jacobs, B.F. Sels, Ternary Ag/MgO-SiO $_2$ Catalysts for the Conversion of Ethanol into Butadiene, ChemSusChem. 8 (2015) 994–1008, https://doi.org/10.1002/cssc.201402894.
[15] M.D. Jones, Catalytic transformation of ethanol into 1,3-butadiene, Chem. Cent. J. 8 (2014) 1–5, https://doi.org/10.1186/s13065-014-0053-4.
[16] G. Natta, R. Rigamonti, Synthesis of butadiene from ethyl alcohol. Thermodynamic studies and the specific function of catalysts, Chim. Ind. 29 (1947) 195–200.
[17] V.L. Sushkevich, I.I. Ivanova, V.V. Ordomsky, E. Taarning, Design of a Metal-Promoted Oxide Catalyst for the Selective Synthesis of Butadiene from Ethanol, ChemSusChem. 7 (2014) 2527–2536, https://doi.org/10.1002/cssc.201402346.
[18] V.L. Sushkevich, I.I. Ivanova, S. Tolborg, E. Taarning, Meerwein-Ponndorf-Verley-Oppenauer reaction of crotonaldehyde with ethanol over Zr-containing catalysts, J. Catal. 316 (2014) 121–129, https://doi.org/10.1016/j.jcat.2014.04.019.
[19] G. Pomalaza, P. Arango Ponton, M. Capron, F. Dumeignil, Ethanol-to-butadiene: the reaction and its catalysts, Catal. Sci. Technol. 10 (2020) 4860–4911, https://doi.org/10.1039/d0cy00784f.
[20] H.E. Jones, E.E. Stahly, B.B. Corson, Butadiene from Ethanol. Reaction mechanism, J. Am. Chem. Soc. 71 (1949) 1822–1828, https://doi.org/10.1021/ja01173a084.
[21] W.J. Toussaint, J.T. Dunn, United States, US2421361, 1947.
[22] B.B. Corson, H.E. Jones, C.E. Welling, J.A. Hinckley, E.E. Stahly, Butadiene from ethyl alcohol. Catalysis in the one-and two-stop processes, Ind. Eng. Chem. 42 (1950) 359–373, https://doi.org/10.1021/ie50482a039.
[23] M.D. Jones, C.G. Keir, C. Di Iulio, R.A.M. Robertson, C.V. Williams, D.C. Apperley, Investigations into the conversion of ethanol into 1,3-butadiene, Catal. Sci. Technol. 1 (2011) 267, https://doi.org/10.1039/c0cy00081g.
[24] V.V. Ordomsky, V.L. Sushkevich, I.I. Ivanova, Study of acetaldehyde condensation chemistry over magnesia and zirconia supported on silica, J. Mol. Catal. A Chem. 333 (2010) 85–93, https://doi.org/10.1016/j.molcata.2010.10.001.
[25] G. Yang, L. Wang, H. Jiang, Zr-Incorporating SBA-15 for conversion of the ethanol-acetaldehyde mixture to butadiene, React. Chem. Eng. 5 (2020) 1833–1844, https://doi.org/10.1039/d0re00160k.
[26] W.J. Toussaint, J.T. Dunn, D.R. Jachson, Production of butadiene from alcohol, Ind. Eng. Chem. 39 (1947) 120–125, https://doi.org/10.1021/ie50446a010.
[27] H. Chae, T. Kim, Y. Moon, H. Kim, K. Jeong, C. Kim, S. Jeong, Applied Catalysis B: Environmental Butadiene production from bioethanol and acetaldehyde over tantalum oxide-supported ordered mesoporous silica catalysts, Appl. Catal. B Environ. 150–151 (2014) 596–604, https://doi.org/10.1016/j.apcatb.2013.12.023.
[28] P.I. Kyriienko, O.V. Larina, S.O. Soloviev, S.M. Orlyk, S. Dzwigaj, High selectivity of TaSiBEA zeolite catalysts in 1,3-butadiene production from ethanol and acetaldehyde mixture, Catal. Commun. 77 (2016) 123–126, https://doi.org/10.1016/j.catcom.2016.01.023.
[29] J.L. Cheong, Y. Shao, S.J.R. Tan, X. Li, Y. Zhang, S.S. Lee, Highly active and selective Zr/MCF catalyst for production of 1,3-Butadiene from ethanol in a dual fixed bed reactor system, ACS Sustain. Chem. Eng. 4 (2016) 4887–4894, https://doi.org/10.1021/acssuschemeng.6b01193.
[30] M. Gao, M. Zhang, H. Jiang, 1,3-Butadiene production from bioethanol and acetaldehyde over zirconium oxide supported on series silica catalysts, Catal. Surv. Asia. 22 (2018) 118–122, https://doi.org/10.1007/s10563-018-9243-8.
[31] M. Gao, H. Jiang, M. Zhang, Conversion of ethanol and acetaldehyde to 1, 3-butadiene catalyzed by Zr–Si materials, Catal. Surv. Asia. 22 (2018) 222–229, https://doi.org/10.1007/s10563-018-9254-5.
[32] Y. Xu, Z. Liu, Z. Han, M. Zhang, Ethanol/acetaldehyde conversion into butadiene over sol–gel ZrO $_2$ –SiO $_2$ catalysts doped with ZnO, RSC Adv. 7 (2017) 7140–7149, https://doi.org/10.1039/C6RA25139K.
[33] X. Li, J. Pang, C. Wang, L. Li, X. Pan, M. Zheng, T. Zhang, Conversion of ethanol to 1,3-butadiene over high-performance Mg-ZrO: X/MFI nanosheet catalysts via the two-step method, Green Chem. 22 (2020) 2852–2861, https://doi.org/10.1039/d0gc00290a.
[34] Z. Han, X. Li, M. Zhang, Z. Liu, M. Gao, Sol–gel synthesis of ZrO $_2$ –SiO $_2$ catalysts for the transformation of bioethanol and acetaldehyde into 1,3-butadiene, RSC Adv. 5 (2015) 103982–103988, https://doi.org/10.1039/C5RA22623F.
[35] A. Klein, K. Keisers, R. Palkovits, Formation of 1,3-butadiene from ethanol in a two-step process using modified zeolite-β catalysts, Appl. Catal. A Gen. 514 (2016) 192–202, https://doi.org/10.1016/j.apcata.2016.01.026.
[37] B.B. Corson, E.E. Stahly, H.E. Jones, H.D. Bishop, Butadiene from ethyl alcohol, study of the variables of operation, Ind. Eng. Chem. 41 (1949) 1012–1017.
[38] J.V. Ochoa, C. Bandinelli, O. Vozniuk, A. Chieregato, A. Malmusi, C. Recchi, F. Cavani, An analysis of the chemical, physical and reactivity features of MgO–SiO $_2$ catalysts for butadiene synthesis with the Lebedev process, Green Chem. 18 (2016) 1653–1663, https://doi.org/10.1039/C5GC02194D.

[39] P.I. Kyriienko, O.V. Larina, S. Dzwigaj, S.O. Soloviev, S.M. Orlyk, Effect of the composition of ethanol–water mixtures on the properties of oxide (Zn-Zr-Si) and zeolitic (Ta/SiBEA) catalysts in the production of 1,3-butadiene, Theor. Exp. Chem. 55 (2019) 266–273, https://doi.org/10.1007/s11237-019-09618-1.
[40] O.V. Larina, I.M. Remezovskyi, P.I. Kyriienko, S.O. Soloviev, S.M. Orlyk, 1,3-Butadiene production from ethanol–water mixtures over Zn–La–Zr–Si oxide catalyst, React. Kinet. Mech. Catal. 127 (2019) 903–915, https://doi.org/10.1007/s11144-019-01618-5.
[41] P.I. Kyriienko, O.V. Larina, S.O. Soloviev, S.M. Orlyk, Catalytic conversion of ethanol into 1,3-Butadiene: achievements and prospects: a review, Theor. Exp. Chem. 56 (2020) 213–242, https://doi.org/10.1007/s11237-020-09654-2.
[42] O.V. Larina, N.D. Shcherban, P.I. Kyriienko, I.M. Remezovskyi, P.S. Yaremov, I. Khalakhan, G. Mali, S.O. Soloviev, S.M. Orlyk, S. Dzwigaj, Design of effective catalysts based on ZnLaZrSi oxide systems for obtaining 1,3-Butadiene from aqueous ethanol, ACS Sustain. Chem. Eng. 8 (2020) 16600–16611, https://doi.org/10.1021/acssuschemeng.0c05925.
[43] G.M. Cabello González, P. Concepción, A.L. Villanueva Perales, A. Martínez, M. Campoy, F. Vidal-Barrero, Ethanol conversion into 1,3-butadiene over a mixed Hf-Zn catalyst: effect of reaction conditions and water content in ethanol, Fuel Process. Technol. 193 (2019) 263–272, https://doi.org/10.1016/j.fuproc.2019.04.036.
[44] P.I. Kyriienko, O.V. Larina, D.Y. Balakin, A.O. Stetsuk, Y.M. Nychiporuk, S. O. Soloviev, S.M. Orlyk, 1,3-Butadiene production from aqueous ethanol over ZnO/MgO-SiO2 catalysts: insight into H2O effect on catalytic performance, Appl. Catal. A Gen. 616 (2021) 118081, https://doi.org/10.1016/j.apcata.2021.118081.
[45] W.M. Quattlebaum, W.J. Toussaint, J.T. Dunn, Deoxygenation of certain aldehydes and ketones: preparation of butadiene and styrene, J. Am. Chem. Soc. 69 (1947) 593–599, https://doi.org/10.1021/ja01195a040.
[46] G.M. Cabello González, R. Murciano, A.L. Villanueva Perales, A. Martínez, F. Vidal-Barrero, M. Campoy, Ethanol conversion into 1,3-butadiene over a mixed Hf-Zn catalyst: a study of the reaction pathway and catalyst deactivation, Appl. Catal. A Gen. 570 (2019), https://doi.org/10.1016/j.apcata.2018.11.010.
[47] G.O. Ezinkwo, V.F. Tretjakov, R.M. Talyshinky, A.M. Ilolov, T.A. Mutombo, Creation of a continuous process for bio-ethanol to butadiene conversion via the use of a process initiator, Catal. Commun. 43 (2014) 207–212, https://doi.org/10.1016/j.catcom.2013.10.015.
[48] V.F. Tret'yakov, R.M. Talyshinskii, A.M. Ilolov, A.L. Maksimov, S.N. Khadzhiev, Initiated conversion of ethanol to divinyl by the lebedev reaction, Pet. Chem. 54 (2014) 195–206, https://doi.org/10.1134/S0965544114020133.
[49] G.M. Cabello González, A.L. Villanueva Perales, M. Campoy, J.R. López Beltran, A. Martínez, F. Vidal-Barrero, Kinetic modelling of the one-step conversion of aqueous ethanol into 1,3-butadiene over a mixed hemimorphite-HfO2/SiO2 catalyst, Fuel Process. Technol. 216 (2021) 106767, https://doi.org/10.1016/j.fuproc.2021.106767.
[50] C. Liu, Y. Li, L. Wu, Z. Geng, Synthesis of 1,3-butadiene from ethanol/acetaldehyde over ZrO2-MgO-SiO2 catalyst: the thermodynamics and reaction kinetics analysis, Chem. Eng. J. 127861 (2020), https://doi.org/10.1016/j.cej.2020.127861.
[51] D. Dussol, N. Cadran, N. Laloue, L. Renaudot, J.M. Schweitzer, New insights of butadiene production from ethanol: Elucidation of concurrent reaction pathways and kinetic study, Chem. Eng. J. (2019), https://doi.org/10.1016/j.cej.2019.123586.
[52] T.W. Kim, J.W. Kim, S.Y. Kim, H.J. Chae, J.R. Kim, S.Y. Jeong, C.U. Kim, Butadiene production from bioethanol and acetaldehyde over tantalum oxide-supported spherical silica catalysts for circulating fluidized bed, Chem. Eng. J. 278 (2015) 217–223, https://doi.org/10.1016/j.cej.2014.09.110.
[53] C.A. Emeis, Determination of integrated molar extinction coefficients for infrared absorption bands of pyridine adsorbed on solid acid catalysts, J. Catal. 141 (1993) 347–354, https://doi.org/10.1006/JCAT.1993.1145.
[54] A. Chieregato, J.V. Ochoa, C. Bandinelli, G. Fornasari, F. Cavani, M. Mella, On the chemistry of ethanol on basic oxides: revising mechanisms and intermediates in the lebedev and guerbet reactions, ChemSusChem. 8 (2015) 377–388, https://doi.org/10.1002/cssc.201402632.
[55] L. Qi, Y. Zhang, M.A. Conrad, C.K. Russell, J. Miller, A.T. Bell, Ethanol conversion to butadiene over isolated zinc and yttrium sites grafted onto dealuminated beta zeolite, J. Am. Chem. Soc. 142 (2020) 14674–14687, https://doi.org/10.1021/jacs.0c06906.
[56] T. Yan, L. Yang, W. Dai, C. Wang, G. Wu, N. Guan, M. Hunger, L. Li, W. Dai, L. Li, T. Yan, G. Wu, C. Wang, N. Guan, On the deactivation mechanism of zeolite catalyst in ethanol to butadiene conversion, J. Catal. 367 (2018) 7–15, https://doi.org/10.1016/j.jcat.2018.08.019.
[57] C.D. Knightes, C.A. Peters, Statistical analysis of nonlinear parameter estimation for Monod biodegradation kinetics using bivariate data, Biotechnol. Bioeng. 69 (2000) 160–170, https://doi.org/10.1002/(SICI)1097-0290(20000720)69:2<160::AID-BIT5>3.0.CO;2-J.
[58] H.S. Fogler, Elements of Chemical Reaction Engineering, 6th ed, Prentice Hall, 2020.
[59] F.D. Marques-Marinho, I.A. Reis, C.D. Vianna-Soares, Construction of analytical curve fit models for simvastatin using ordinary and weighted least squares methods, J. Braz. Chem. Soc. 24 (2013) 1469–1477, https://doi.org/10.5935/0103-5053.20130187.
[60] K.J. N, H. Yamazaki, A. Ishikawa, R. Osuga, S. Takao, T. Yokoi, S. Kikkawa, K. Teramura, T. Tanaka, Monolayer tantalum oxide on mesoporous silica substrate, Chem. Select. 1 (2016) 3124–3131, https://doi.org/10.1002/slct.201600507.
[61] Y. Chen, J.L.G. Fierro, T. Tanaka, I.E. Wachs, Supported tantalum oxide catalysts: synthesis, physical characterization, and methanol oxidation chemical probe reaction, J. Phys. Chem. B 107 (2003) 5243–5250, https://doi.org/10.1021/jp0276451.
[62] M. Baltes, A. Kytökivi, B.M. Weckhuysen, R.A. Schoonheydt, P. Van Der Voort, E. F. Vansant, Supported tantalum oxide and supported vanadia-tantala mixed oxides: structural characterization and surface properties, J. Phys. Chem. B 105 (2001) 6211–6220, https://doi.org/10.1021/jp010628b.
[63] F. Tielens, T. Shishido, S. Dzwigaj, What do tantalum framework sites look like in zeolites? A combined theoretical and experimental investigation, J. Phys. Chem. C 114 (2010) 9923–9930, https://doi.org/10.1021/jp102181m.
[64] G. Pomalaza, P. Simon, A. Addad, M. Capron, F. Dumeignil, Properties and activity of Zn-Ta-TUD-1 in the Lebedev process, Green Chem. 22 (2020) 2558–2574, https://doi.org/10.1039/d0gc00103a.
[65] M. Zhang, X. Tan, T. Zhang, Z. Han, H. Jiang, The deactivation of a ZnO doped ZrO2-SiO2 catalyst in the conversion of ethanol/acetaldehyde to 1,3-butadiene, RSC Adv. 8 (2018) 34069–34077, https://doi.org/10.1039/c8ra06757k.
[66] N.R. Draper, H. Smith, Applied Regression Analysis, John Wiley & Sons, 1998.